NURETH14-418

RELAP5 ANALYSIS OF TWO-PHASE DECOMPRESSION AND RAREFACTION WAVE PROPAGATION UNDER A TEMPERATURE GRADIENT

Nathan Lafferty, Victor H. Ransom, Martin Lopez de Bertodano¹
School of Nuclear Engineering, Purdue University, West Lafayette, Indiana 47907
Nathan.Lafferty@nrc.gov, ransom@ecn.purdue.edu, bertodan@purdue.edu

Abstract

The capability of RELAP5 to model single and two-phase acoustic waves is demonstrated with the use of fine temporal and spatial discretizations. Two cases were considered: a single phase air shock tube problem and pressure waves observed by Takeda and Toda in a two-phase decompression experiment in a pipe.

Whereas the agreement for the single phase case is excellent, some discrepancies were observed in the two-phase case. However, RELAP5 produced markedly better results after adjusting the bubble size and the choked flow area. These results illustrate the need of a dynamic model for the interfacial area concentration (i.e., the bubble size).

Introduction

Acoustic wave propagation phenomena are of key interest in the field of nuclear reactor safety. To understand the forces on internal reactor components it is necessary to analyze fluid pressure behavior immediately after a postulated LOCA [1]. Such an analysis provides insight into possible structural damage resulting in a failure to maintain core geometry and core cooling. In the event of a LOCA in a water cooled reactor, the subcooled blowdown results in the propagation of a rarefaction wave [1]. The wave eventually travels from the point of the break through the coolant piping to the nuclear reactor's core region. Furthermore, a temperature gradient in the core leads to unique behavior of the rarefaction wave.

Edwards and O'Brien [1] compared numerical simulations which track the initial rarefaction wave and related void formation following the bursting of a pressurized horizontal subcooled pipe of constant temperature with experimental results [1]. The data from Edwards and O'Brian has been used to validate the two-fluid model RELAP5 computer code [3]. Later, Takeda and Toda [2] experimentally observed the pressure behavior in a vertical pipe under a temperature gradient and analyzed it with simple equilibrium and non-equilibrium wave propagation models. Takeda and Toda show that for a pipe with a temperature gradient, flashing in the hotter section results from the passing of a rarefaction wave with a large enough amplitude; whereas, the colder section, with a lower vapor pressure, remains subcooled liquid. A large discontinuity in the sound speed arises between the two-phase and single-phase regions serving as a reflective surface. The data from Takeda and Toda has never been compared with a RELAP5 simulation.

¹ Corresponding author

The RELAP5 computer code, widely used in nuclear reactor transient analysis, employs a two fluid model consisting of the mass, momentum, and energy conservation equations for each phase solved using a semi-implicit finite-difference technique [3]. Tiselj and Cerne [4] have shown that RELAP5 is capable of tracking acoustic waves with almost second-order accuracy with the use of small time step in a simulation of a two-phase shock tube and water hammer analysis benchmarked with experimental data.

This work consists of three parts: First, the application of RELAP5/MOD3.3 Patch03 to model an air filled shock tube (i.e. Riemann's problem) at very small time steps and a refined grid to demonstrate the capability of RELAP5 to resolve single phase acoustic waves accurately. Secondly, the RELAP5 simulation of the experiment carried out by Takeda and Toda to investigate the capability of RELAP5 to resolve two-phase acoustic waves. In particular, the effect of thermal non-equilibrium and the constitutive relation for the bubble size will be analyzed. The last part is a brief discussion of the stability of the RELAP5 two-fluid model.

1. Air Shock Tube

A frictionless shock tube was investigated using the RELAP5/MOD3.3 code to validate it for single-phase wave propagation. The corresponding simplified one-dimensional single-phase continuity and momentum equations are listed below where ρ is density, v is velocity and p is pressure [4]:

$$\frac{\partial \rho}{\partial t} + \frac{\partial \rho v}{\partial x} = 0$$

$$\rho \frac{\partial v}{\partial t} + \frac{\rho}{2} \frac{\partial v^2}{\partial x} + \frac{\partial p}{\partial x} = 0$$
(1)

Tiselj and Cerne derived the following simplified single-phase acoustic wave equations

$$\frac{\partial \rho}{\partial t} + \rho \frac{\partial v}{\partial x} = 0$$

$$\rho \frac{\partial v}{\partial t} + \frac{\partial p}{\partial x} = 0$$
(2)

assuming a negligible fluid velocity and $\delta\rho/\rho$ ratio [4]. These are reasonable assumptions due to the very small density fluctuations and fluid velocity relative to the sonic velocity. Tiselj and Cerne show that when Eqs. (2) are discretized following the RELAP5 procedure, the first order spatial truncation errors vanish [4]

The shock tube model consists of stagnant air separated by a diaphragm shown in Fig. 1. Gas 3 on the left side of the diaphragm is initially at a higher pressure than gas 1. In order to allow an analytical solution the air on each side of the diaphragm has initially the same temperature. The diaphragm is broken creating a right-traveling shock wave and a left-traveling rarefaction wave as shown. The velocity of fluids states 2 and 4 are the same. No entropy change between fluid states 3 and 4 takes place, and entropy increases across the shock from 1 to 2, so the temperatures in fluid states 2 and 4 are different [5].

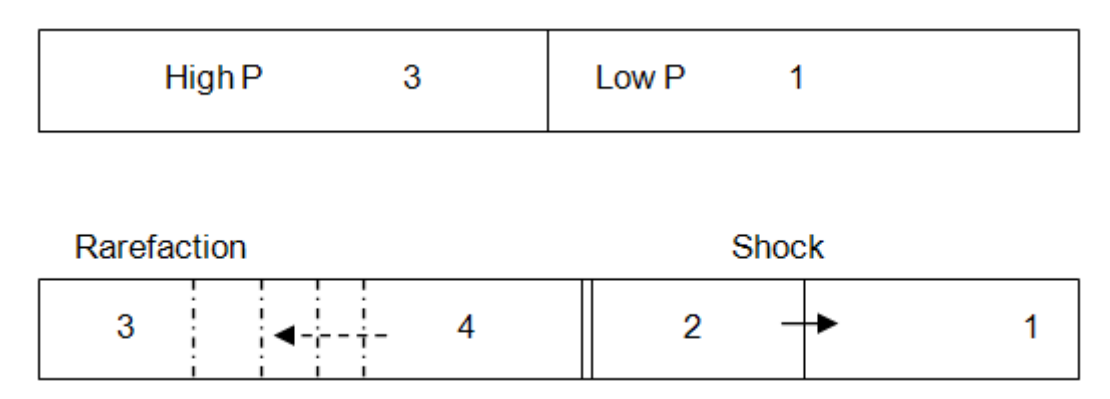


Fig. 1. Schematic of air shock tube.

A 9.9 meter pipe is divided into 99 nodes, each one 0.1 m long. The cross sectional area of the pipe is 0.00456 m^2 (3 inch inner diameter). Tiselj and Cerne recommend short time steps, $\Delta t \approx 0.01 \frac{\Delta x}{c}$, where c is the speed of sound and Δx is the nodal length, in order to trace acoustic waves with almost second-order accuracy [4]. Therefore, the time step was chosen to produce a value of about 0.01 for the acoustic Courant Number. The gas used for this experiment is air at 297 K. Gas 3, to the left of the diaphragm, is initialized at 2 MPa and Gas 1, to the right, is at 1 MPa. The pipe is adiabatic.

Fig. 2 shows the progression of the shock and rarefaction waves in the tube. The dense nodalization and small time step produce results matching the analytic solution. For the analytic solution the air is assumed a perfect gas, which is valid since the ratio of the temperature to the critical temperature is greater than two, and the specific heats are approximately constant due to the minor temperature fluctuations. The pressure of gas 2 calculated by RELAP5 is 1.406 MPa and when compared with the analytic solution [5] of 1.402 MPa produces only 0.29% relative error. Selecting the RELAP5 10 ms data, the shock wave velocity is 400 m/s and has an error of 0.24%. The velocity of gas 2 taken from RELAP5 is 84.12 m/s, and has a 1.7% relative error compared to the analytic value of 84.49 m/s. The behavior of the pressure wave also matches what is predicted. The shock wave has a relatively steep slope that stays steep, while the rarefaction wave spreads as it propagates [5]. The nonphysical numerical oscillations are a byproduct of the reduced time step. Increasing the time step reduces the numerical oscillations but diffuses the steep pressure gradients [4].

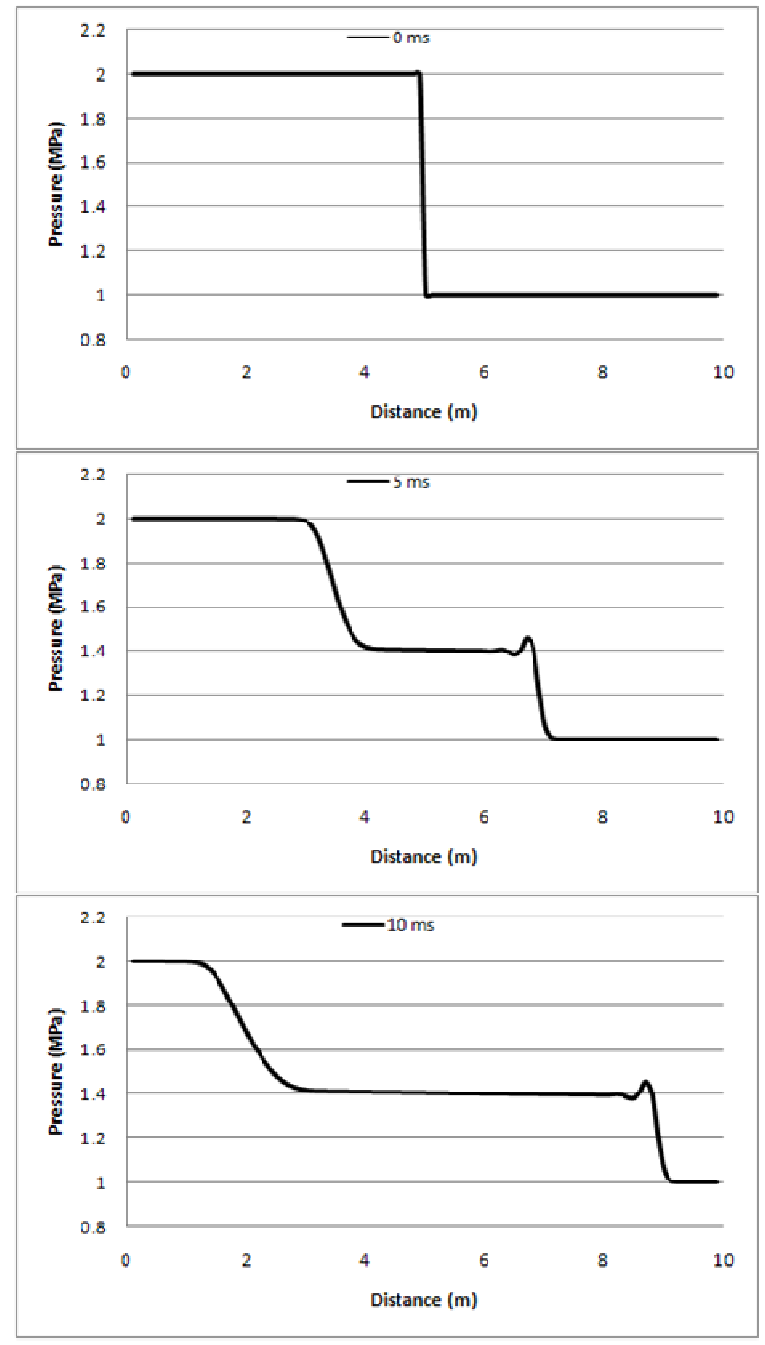


Fig. 2. Pressure distribution in shock tube at 0, 5, and 10 ms.

2. Blowdown Under Temperature Gradient

Takeda and Toda measured pressure oscillations during the decompression of a vertical pipe with a temperature gradient [2]. The pipe may be divided into a two-phase region at the top and a subcooled region in the rest of the pipe.

The RELAP5 one-dimensional two-phase conservation equations governing wave propagation are given below [3],[6].

Conservation of mass:

The 14th International Topical Meeting on Nuclear Reactor Thermalhydraulics, NURETH-14 Toronto, Ontario, Canada, September 25-30, 2011

$$\frac{\partial}{\partial t}(\alpha_{g}\rho_{g}) + \frac{\partial}{\partial x}(\alpha_{g}\rho_{g}v_{g}) = \Gamma_{g}$$

$$\frac{\partial}{\partial t}(\alpha_{f}\rho_{f}) + \frac{\partial}{\partial x}(\alpha_{f}\rho_{f}v_{f}) = -\Gamma_{g}$$
(3)

Conservation of momentum:

$$\frac{\partial(\alpha_{g}\rho_{g}v_{g})}{\partial t} + v_{g} \frac{\partial(\alpha_{g}\rho_{g}v_{g})}{\partial x} = -\alpha_{g} \frac{\partial P}{\partial x} + \alpha_{g}\rho_{g}g - F_{wg} - F_{I} + \Gamma_{g}(v_{I} - v_{g}) - c_{vm}\alpha_{g}\alpha_{f}\rho_{f} \frac{\partial(v_{g} - v_{f})}{\partial t} \\
\frac{\partial(\alpha_{f}\rho_{f}v_{f})}{\partial t} + v_{f} \frac{\partial(\alpha_{f}\rho_{f}v_{f})}{\partial x} = -\alpha_{f} \frac{\partial P}{\partial x} + \alpha_{f}\rho_{f}g - F_{wf} + F_{I} - \Gamma_{g}(v_{I} - v_{f}) - c_{vm}\alpha_{g}\alpha_{f}\rho_{f} \frac{\partial(v_{g} - v_{f})}{\partial t} \tag{4}$$

Where α , ρ , and v are the time and space averaged void fraction, density, and velocity, and the g and f subscripts specify vapor and liquid respectively [6]. Γ_g is the vapor generation. P is the pressure averaged between the two phases [6]. The volumetric wall shear forces experienced by the liquid and vapor are F_{wf} and F_{wg} , respectively, and are equal to zero since the pipe is assumed frictionless [6]. F_I is the volumetric interfacial drag and V_I is the interfacial velocity in the interfacial momentum transfer terms [6]. Finally, the last term on the RHS of Eqs. (4) is the virtual mass force as implemented in RELAP5 and c_{vm} is the virtual mass coefficient. This term has a significant effect on acoustic wave propagation. Eqs. (3) and (4) describe the wave propagation in a two-phase medium. In addition, the two-phase energy conservation equations in RELAP5 are required in order to model the vapor generation that occurs during the depressurization process [3]. Conservation of energy:

$$\frac{\partial}{\partial t}(\alpha_{g}\rho_{g}u_{g}) + \frac{\partial}{\partial x}(\alpha_{g}\rho_{g}u_{g}v_{g}) = -P\frac{\partial\alpha_{g}}{\partial t} - P\frac{\partial}{\partial x}(\alpha_{g}v_{g}) + Q_{ig} + \Gamma_{ig}h_{g}^{*}$$

$$\frac{\partial}{\partial t}(\alpha_{f}\rho_{f}u_{f}) + \frac{\partial}{\partial x}(\alpha_{f}\rho_{f}u_{f}v_{f}) = -P\frac{\partial\alpha_{f}}{\partial t} - P\frac{\partial}{\partial x}(\alpha_{f}v_{f}) + Q_{if} - \Gamma_{ig}h_{f}^{*}$$
(5)

The specific internal energy is represented by u, Q_{ig} and Q_{if} are the interfacial heat transfer terms, Γ_{ig} is the vapor generation resulting from interfacial energy exchange, and h_g^* and h_f^* are the corresponding phasic enthalpies associated with interphase mass transfer[3]. The effects of wall heat transfer and the energy dissipation caused by friction are negligible and omitted in Eqs. (5).

A RELAP5 model was developed for Takeda and Toda's experiment [2]. The water filled pipe has a 53.5 mm inner diameter, a 3.2 m length, and is initially pressurized to 0.855 MPa measured at the top. It contains 99 nodes, each 3.23 cm in length. Fig. 3 shows a diagram of the RELAP5 model. The experimental data [2] was taken at pressure transducers (PT) 3, 4, and 5 which are located at a distance from the break of 0.444, 1.20, and 2.20 m respectively. The volume labeled BC is a time dependent volume representing the atmospheric boundary conditions. The junction representing the break orifice is 15 mm in diameter and is positioned at the top of the test section. It is modeled with an abrupt area change so the code calculates flow losses through the break [3]. A linear temperature distribution is established in the pipe such that the temperature at the base of the pipe is 283.7 K and the temperature at the top is 437.9 K. This temperature distribution produced the greatest pressure oscillations out of the many temperature distributions tested experimentally by Takeda and Toda and will therefore be used in this analysis. Fig. 3 shows the vapor pressure of the water in the pipe based on the initial temperature distribution. The vapor pressure is greatest at the top of the pipe near the postulated break with a value of 0.696 MPa.

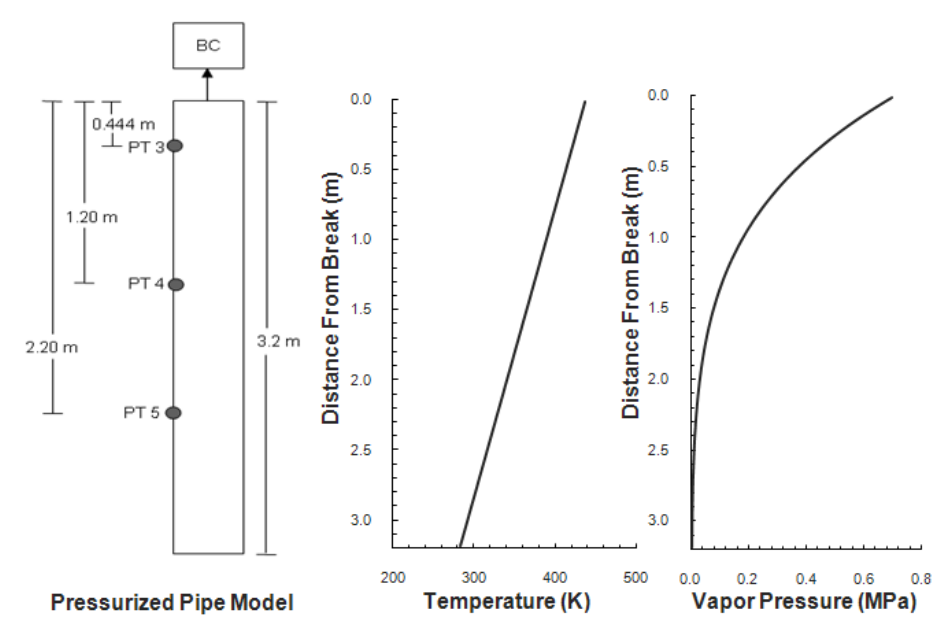


Fig. 3. Model with location of pressure transducers and initial conditions.

Spatial convergence was checked by comparing the 99 node model with a finer 297 node model. Both models produced matching results, therefore the 99 node model was used for further investigations. The effects of adding a heat structure were also investigated and proved negligible, thus confirming the adiabatic assumption. The Ransom-Trapp critical flow model was adopted as it captured the experimental pressure behavior more accurately. A 550 microsecond delay time was applied to the simulated break in order to match the delay in the experiment.

2.1 Thermal Equilibrium Model

The RELAP5 thermal equilibrium option was used in order to provide insight into the depressurization and wave propagation with simplified model assumptions. Fig. 4 shows that the results converge at PT3 as the time step decreases. The results at PT4 and PT5 are similar but they match the data better, so only location PT3 will be shown. The acoustic Courant Numbers 1, 0.1, and 0.01 correspond to a time step value of $\Delta t = \frac{\Delta x}{c}$, $\Delta t = 0.1 \frac{\Delta x}{c}$, and $\Delta t = 0.01 \frac{\Delta x}{c}$ respectively. It is seen that an acoustic Courant Number of 0.1 produces converged results with minimal numerical oscillation that require the least computational effort.

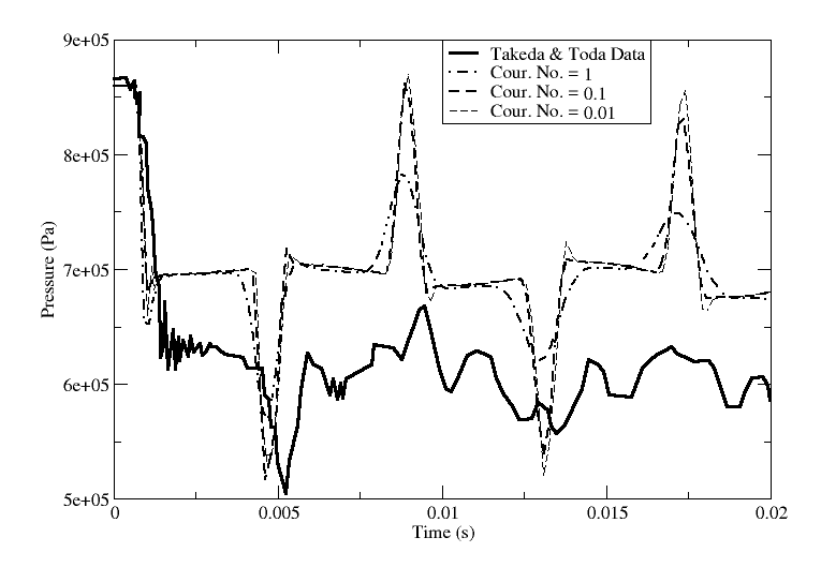


Fig. 4. Thermal equilibrium simulation effect of time step at PT 3.

The RELAP5 simulation with the thermal equilibrium model overpredicts the pressure when compared with the experimental data. A physical explanation for the pressure results calculated with the equilibrium model is that immediately following the pipe rupture, the efflux of fluid through the break leads to a sudden pressure drop to the vapor pressure, 0.696 MPa, at the top of the pipe. Due to the assumption of instantaneous heat transfer between the vapor and liquid, some fluid immediately flashes to steam and a region of low void is formed near the break. This region does not penetrate deep into the pipe. This is because no pressure undershoot occurs. The two-phase region near the pipe break lowers the local speed of sound to approximately 50 m/s and the flow at the break is choked [7]. The pressure in the pipe then stabilizes at the vapor pressure of the fluid and sets the amplitude of the rarefaction wave. The rarefaction wave travels down the pipe, reflects off the closed end as another rarefaction wave of equal strength propagates back toward the top of the pipe where the two-phase region exists, as seen in Fig. 5. Fig. 5 shows a 2D shaded contour plot of the pressure. A line separating two regions of uniform color represents a characteristic line and displays the propagation of the wave front.

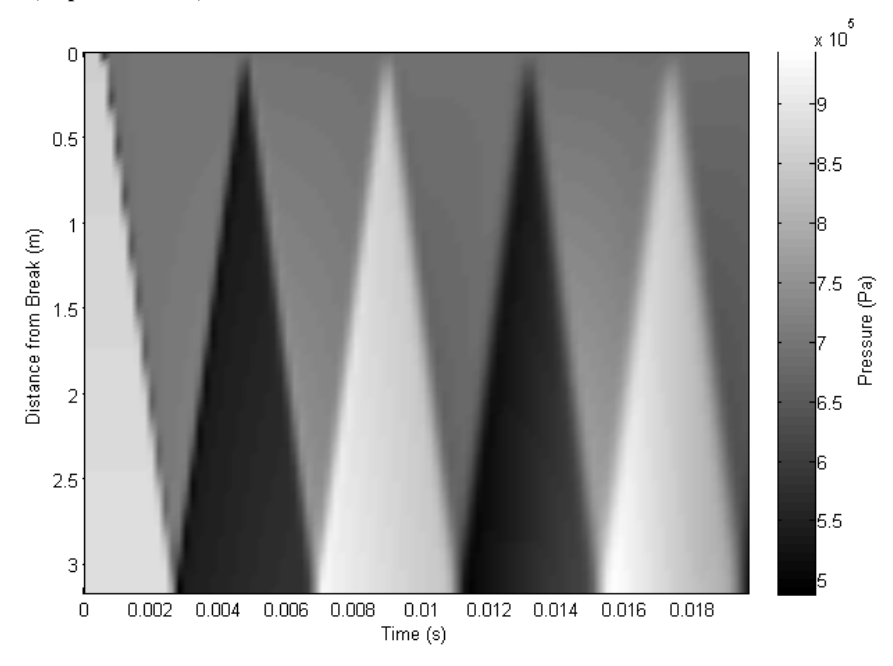


Fig. 5. Thermal equilibrium simulation pressure (Pa) distribution with time.

The rarefaction wave is reflected by the discontinuity in the sound speed, from 1500 m/s to 50 m/s, at the boundary between the single and two-phase flow regions. According to wave propagation theory the reflection and transmission of a wave at an interface with a change in the sound speed [8] is given by

$$A_{R} = \frac{\mu - 1}{\mu + 1} A_{I}$$

$$A_{T} = \frac{2\mu}{\mu + 1} A_{I}$$

$$\mu = \frac{c_{T}}{c_{I}}$$
(6)

Where A_R , A_T , and A_I are the amplitude of the reflected, transmitted and incident wave, respectively. The speed of sound on the transmission side of the interface is c_T and on the incident side is c_I [8]. Due to the very small value for the speed of sound in the two-phase mixture compared to the speed of sound of the liquid, μ is approximately zero. Therefore, the amplitude of the reflected wave is nearly the same as the incident wave and opposite in sign, which matches the wave behavior simulated by RELAP5 at the two-phase interface described above. The two-phase region can also be viewed as a constant pressure boundary because as the wave interacts with it, the two-phase region's smaller bulk modulus volumetrically adjusts with little change in pressure. This will cause the wave to be reflected in an opposite sense with a magnitude similar to that of the incident wave.

Fig. 6 shows the interaction of the rarefaction wave with the vapor pressure established by the temperature gradient. The moment the local pressure drops to the vapor pressure, due to the progression of the rarefaction wave, vaporization occurs and the pressure stays at saturation value without dropping below it. The wave then reflects off the already established two-phase region collapsing the newly voided region and progresses back down the pipe as a compression wave. Minor dispersion, diffusion, and dissipation of the wave is seen in Fig. 5. By understanding the simplified

case of thermal equilibrium, insight is obtained into the importance of non-equilibrium effects caused by interfacial energy transfer and delayed nucleation.

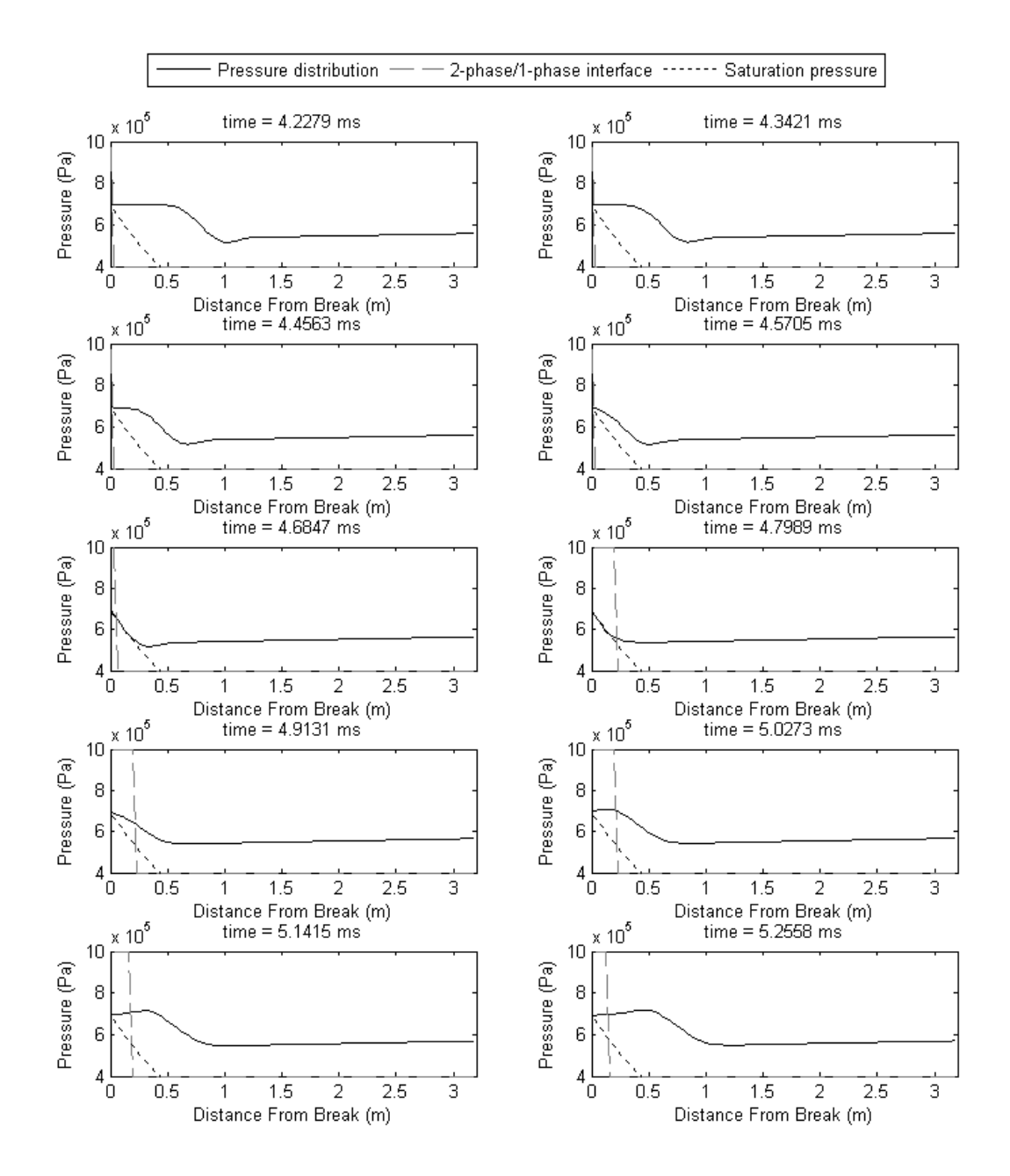


Fig. 6. Thermal equilibrium simulation showing interaction of rarefaction wave with temperature gradient and subsequent voiding.

2.2 Default Thermal Non-equilibrium Model

By default RELAP5 takes into account thermal non-equilibrium (i.e., two energy equations). In particular the default model employs the interfacial mass transfer term for boiling and flashing given by

Eq. (8) which will be discussed in section 2.3.2. Fig. 7 shows the convergence of the default model by reducing the time step. As the time step decreases the pressure gradients steepen; however, with a very small time step nonphysical numerical oscillations emerge at the pressure discontinuities. Reducing the time step also results in a more accurate integration of the interphase mass, energy, and momentum transfer terms [4].

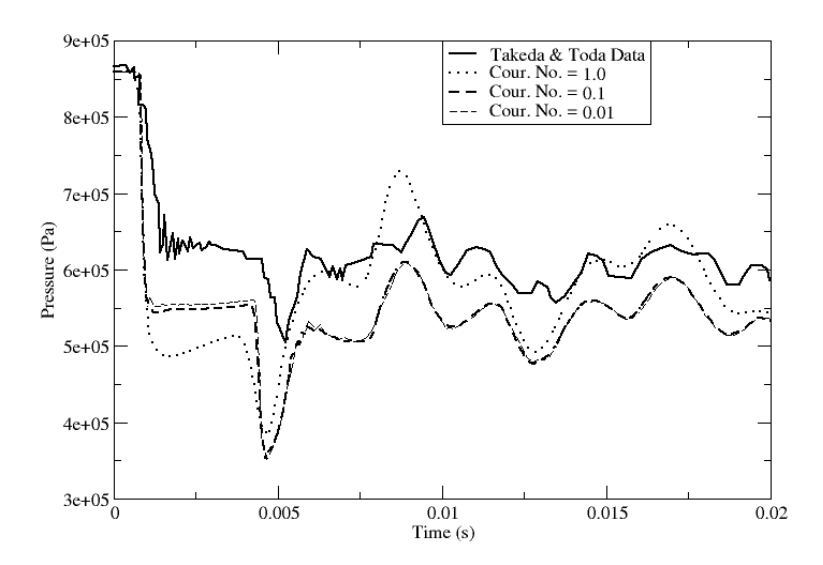


Fig. 7. Default simulation effect of time step at PT 3.

The default simulation results match the experimental behavior of the rarefaction wave better than the equilibrium model. However, RELAP5 predicted a larger initial pressure undershoot as seen in Fig. 7 around 1 ms, and continued to underpredict the pressure throughout the remaining 20 ms at PT 3. The steeper pressure drop curve predicted by RELAP5 denotes an overestimation of the pressure drop rate compared to the experimental data. RELAP5 calculates the propagation velocities of the wave through the subcooled fluid with great accuracy. The default simulation results show the attenuation of the wave amplitude and dispersion of the wave during propagation comparable to the experimental data.

Fig. 8 displays the pressure along the pipe length for the duration of the transient in a three-dimensional plot. The experimental data from Takeda and Toda is superimposed on the plot at the locations of the three pressure transducers. The initial pressure drop down to about 0.55 MPa is shown, with a 0.15 MPa pressure undershoot, as the rarefaction wave travels down the pipe. The wave is reflected off the closed end in a like sense, and travels back toward the top of the pipe as another rarefaction wave with an amplitude similar to that of the incident wave. Fig. 9 displays a contour plot that shows the sound speed distribution in the pipe around 5 ms. Fig. 10 displays a contour plot for the pressure showing the wave characteristic as it reflects off the solid boundary at the bottom and the two-phase region at the top of the pipe.

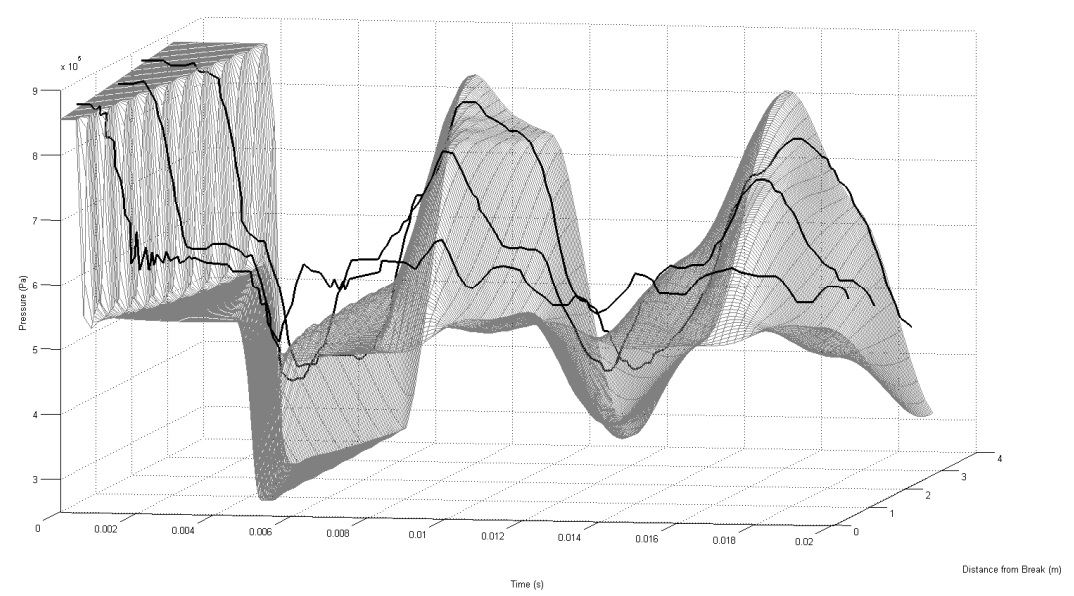


Fig. 8. 3D pressure plot using default simulation compared with experimental data (2).

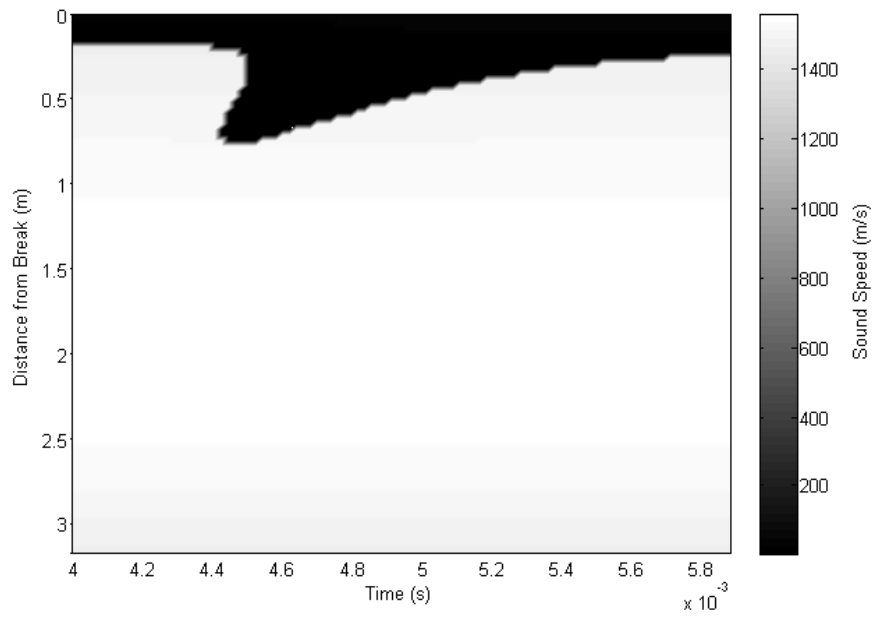


Fig. 9. Default simulation sound speed (m/s) distribution with time.

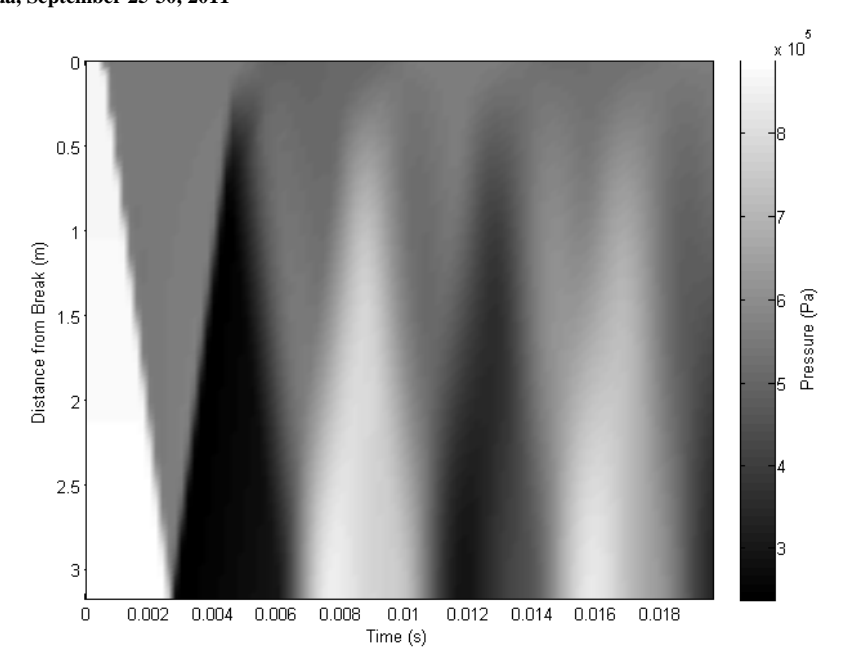


Fig. 10. Default simulation pressure (Pa) distribution with time.

When the rupture occurs, the pressure at the top of the pipe drops below saturation due to thermal non-equilibrium and delayed nucleation. Upon nucleation the pressure levels off below the vapor pressure by the amount $p_{undershoot}$, and this pressure drop propagates down the pipe in the form of a decompression or rarefaction wave. The rarefaction wave reflects off the solid boundary at the bottom of the pipe and doubles back toward the top of the pipe. At approximately 4.5 ms the rarefaction wave returns to the top of the pipe and the region of two-phase flow is suddenly extended from about 0.2 m to about 0.7 m down into the pipe, as shown in Fig. 9. This occurs due to the interaction of the rarefaction wave with the axially decreasing vapor pressure imposed by the initial temperature gradient shown in Fig. 3. Figs. 11 and 12 illustrate the conditions in the pipe as the rarefaction wave travels toward the two-phase layer on top. The reflected rarefaction wave causes the local pressure to drop below the vapor pressure, the fluid is put in tension $p_{tension}$, and voiding begins as shown in Fig. 12. The value of $p_{tension}$ is determined by the delay in nucleation and non-equilibrium effects. In Fig. 13 the dotted line represents the vapor pressure, the solid line the pressure distribution and rarefaction wave, and the dashed grey line shows the boundary between the two-phase and single-phase fluid regions. The figure at 4.4563 ms shows that a separated region of two-phase fluid resembling Fig. 12 forms for a brief moment, surrounded on both sides by single-phase fluid. This can also be observed in Fig. 9. As the rarefaction wave moves on it is then reflected off the initial two-phase region, created by the passing of the first rarefaction wave and it is trapped in the two-phase region that it formed in its wake that extends to 0.7 m. Once caught, the wave then disperses because it takes a long time to pass through the two-phase region. Furthermore, the two-phase sound speed in the region is heterogeneous. The figure at 4.5705 ms demonstrates the non-equilibrium and delayed nucleation effects as the fluid pressure drops below the vapor pressure. The dispersion of the wave is visible in Figs. 10 and 13. Fig. 10 shows that the pressure discontinuity is initially abrupt, but after the interaction of the wave with the two-phase region at 4.5 ms, the pressure discontinuity spreads out as shown by the blurring of the color contours. Later on the effects of dispersion toward the end of the transient even cause a pressure bifurcation as the waves interact. The dissipation of the wave amplitude is also very significant. Therefore, this unique phenomenon of wave entrapment in the two-phase region caused by non-equilibrium and delayed nucleation is what determines the wave to be smeared out.

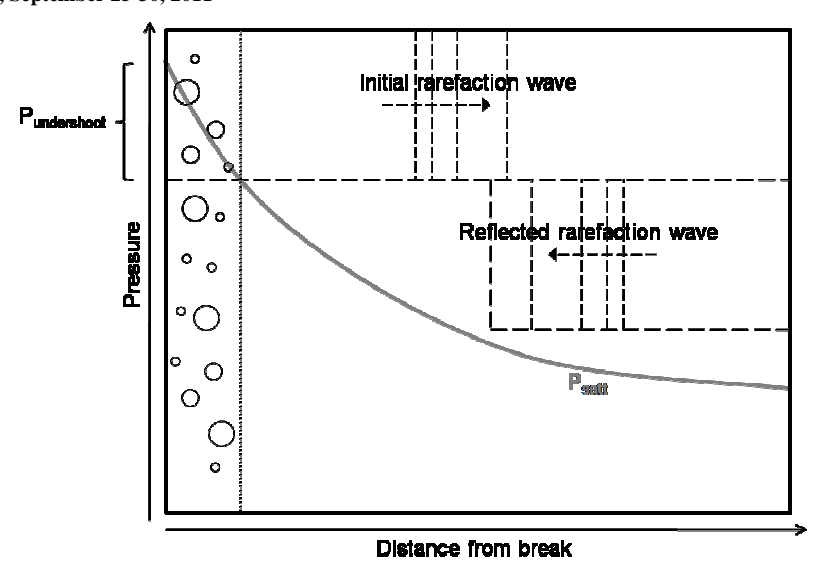


Fig. 11. Initial pressure drop creating two-phase region and rarefaction wave reflection.

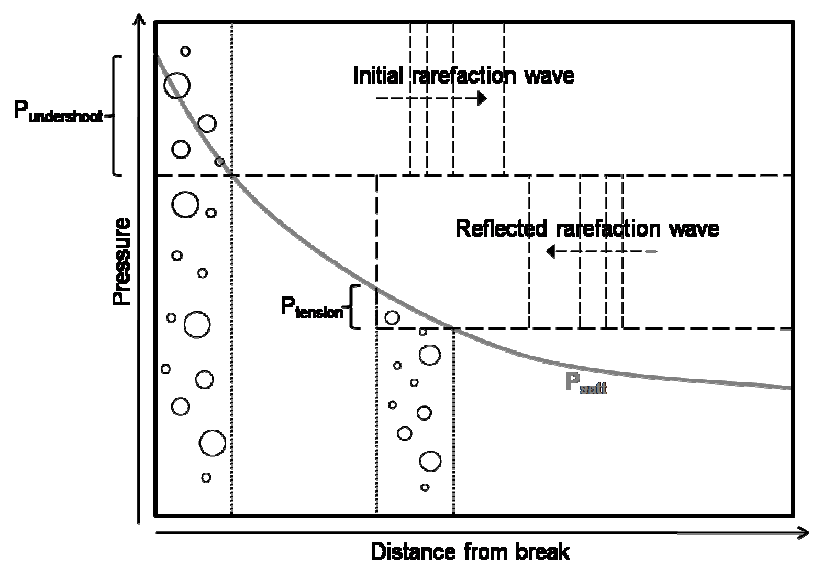


Fig. 12. Interaction of reflected rarefaction wave with temperature gradient.

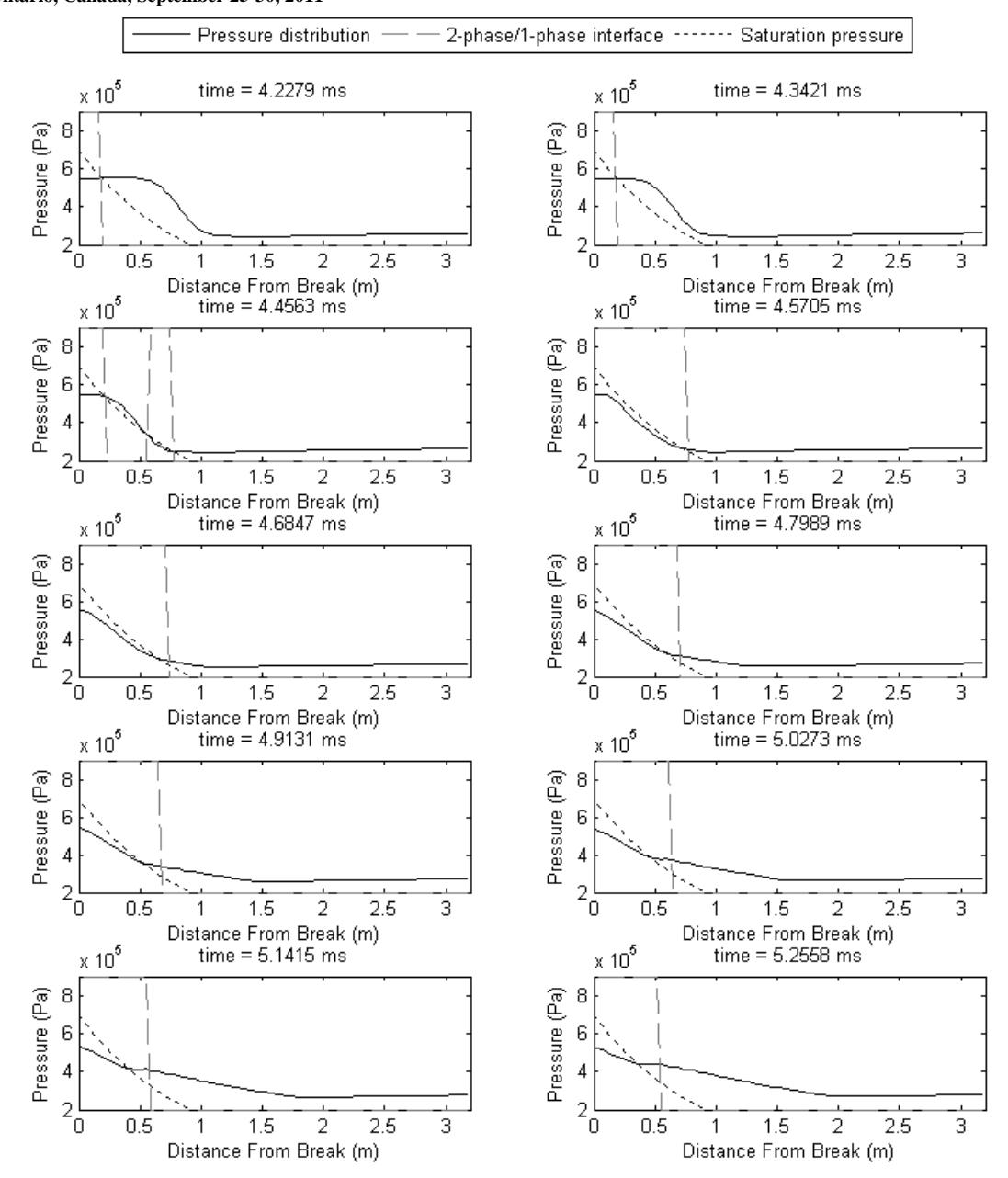


Fig. 13. Default simulation showing interaction of rarefaction wave with temperature gradient and subsequent voiding.

2.3 Discussion

2.3.1 Choked Flow Model

The overprediction of the initial pressure undershoot seen in the RELAP5 default simulation could be due to a variety of uncertainties. First, for subcooled conditions the Ransom-Trapp critical flow model [9] may overpredict the break flow. Second, for an orifice geometry, which is used as the break in the Takeda and Toda experiment, the discharge coefficient is generally reduced. In the third place the

RELAP5 calculation of the pressure undershoot depends on the initial pressure drop rate. The Alamgir and Lienhard correlation [10] used in RELAP5 is only applicable when the pressure drop rate is between 0.004 and 1.803 Matm/s. Using the initial pressure drop at PT 3 from the experimental data of Takeda and Toda the rate of depressurization is about 0.002 Matm/s. A more mechanistic model involving direct analysis of permanent gas pockets, surface geometry, and contact angles would be needed [10] for RELAP5 to make a more accurate prediction of the undershoot. Finally, the break in the Takeda and Toda experiment involved the rupture of a Mylar disk, and fragments could remain and obstruct the flow resulting in a smaller break area. The subcooled discharge coefficient for the Ransom-Trapp critical flow model may be adjusted in order to adjust the pressure undershoot. The discharge coefficient is a user-specified parameter to correct for uncertainties caused by break geometries and the critical flow model. It is multiplied by the throat area and is equivalent to adjusting the break area.

Fig. 14 shows the effect of the subcooled discharge coefficient at PT 3. The discharge coefficient values of 0.25, 0.5, 0.75, and 1.0 (default simulation) are compared with the experimental data. It is shown that a discharge coefficient of 0.5 produces the best agreement with the pressure undershoot observed in the experiment. After reflecting off the two-phase region at around 5 ms, the compression wave's amplitude is also reduced. Although the discharge coefficient can set a pressure undershoot that matches the experimental data, the pressure drop rate remains unchanged so the initial rarefaction wave still has a steeper slope than the slope seen experimentally.

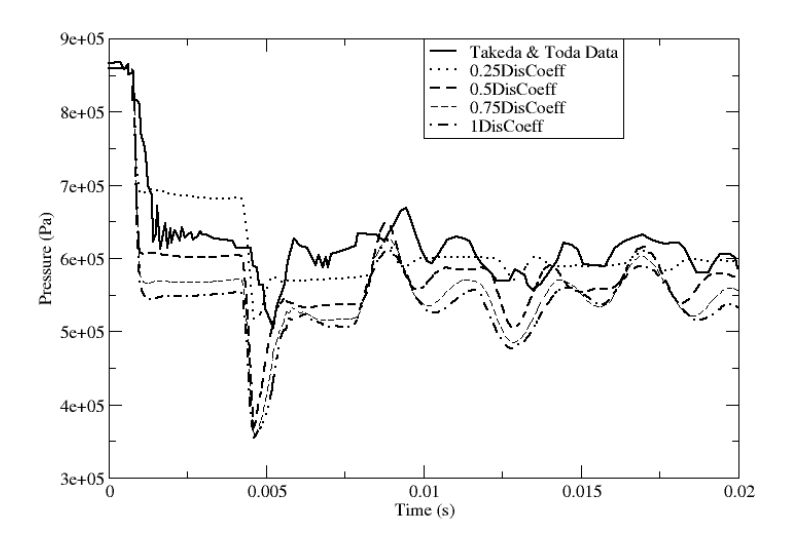


Fig. 14. Effect of discharge coefficient at PT 3.

2.3.2 Interfacial Heat and Mass Transfer

A thorough study of the physical mechanism that controls bubble formation and growth is needed in order to determine the bulk interfacial heat transfer model. Increased bubble growth would result in a pressure increase tending toward equilibrium at a faster rate. During the entire depressurization period under investigation, 20 ms, the fluid remains in the bubbly flow regime. Also, due to the pressure undershoot the fluid is a superheated liquid resulting in vaporization and heat transfer from the fluid to the bubble interface. It should be noted that the liquid superheat for nucleation in the present case is determined by the Alamgir and Lienhard correlation [10], far from the spinodal limit prescribed by the steam tables of RELAP5. The temperature of the forming vapor is equal to saturation temperature. The corresponding liquid interfacial heat transfer is investigated for the case of a bubbly superheated liquid. The liquid interfacial heat transfer term [3] shown in Eqs. (5) is calculated as

$$Q_{if} = h_{if} a_{gf} (T^s - T_f) \tag{7}$$

The variable T^s denotes saturation temperature, T_f is the liquid temperature, h_{if} is the liquid interfacial heat transfer coefficient, and a_{gf} is the interfacial area per unit volume. The volumetric mass vaporization rate at the interface [3] assuming negligible heat transfer from the vapor to the bubble interface is

$$\Gamma_{ig} = -\left[\frac{h_{if}a_{gf}(T^s - T_f)}{h_g^s - h_f}\right] \tag{8}$$

where h_g^s and h_f are the specific enthalpies of the vapor at saturation and the liquid respectively. The underlying parameter to be adjusted that dictates the energy transfer between the phases, hence the rate of vaporization, is the interfacial area per unit volume [3]. In terms of the average diameter, d_b , it is given by

$$a_{gf} = \frac{3.6 \,\alpha_{bub}}{d_b} \tag{9}$$

where $lpha_{\scriptscriptstyle bub}$ depends on the vapor void fraction , $lpha_{\scriptscriptstyle g}$, and is calculated to be

$$\alpha_{bub} = \max(\alpha_{p}, 10^{-5}) \tag{10}$$

The Sauter-mean bubble diameter, d_b , is essential in calculating all energy, mass, and momentum transfer that occur between the two phases. As Eq. (9) shows, the bubble diameter determines the interfacial area concentration, a_{gf} . In RELAP5/MOD3.3 Patch03 the bubble diameter is calculated as a function of the Laplace Length [11],[12]

$$d_b = 2L_o \tag{11}$$

The Laplace Length L_o can be found by

$$L_o = \sqrt{\frac{\sigma}{g(\rho_f - \rho_g)}} \tag{12}$$

where σ is the liquid surface tension and g is the gravitational constant. The bubble diameter is restricted by the bounds 0.1 mm $\leq d_b \leq 0.9d_h$, where d_h is the volume hydraulic diameter [3].

The bubble diameter was adjusted to correct the under-prediction of the pressure using the RELAP5 default simulation. By reducing the bubble diameter, the interfacial area concentration will increase and thus the interfacial heat transfer will increase. This will then cause more vaporization and a slight increase in the pressure. This adjustment was performed by multiplying the Laplace Length, or

bubble radius, by a factor. Fig. 15 shows the effect of multiplying the Laplace Length by a factor of 0.001, 0.1, 0.25, and 1.0 (default simulation) compared with the experimental results. The figures show that as the bubble diameter is reduced, the interfacial area and interfacial heat transfer is increased, and the pressure in the pipe rises. It is important to note that the bubble diameter has no effect on the pressure undershoot during the initial depressurization. That value is determined by the choked flow model. The explanation for the ramp in pressure after the pressure undershoot, around 1 ms, shown in Fig. 15 is that the upper pipe section is initially in tension, see Fig. 23, and is vaporizing faster at that location due to the increased interfacial heat transfer, which then causes the pressure to increase relatively slowly toward equilibrium.

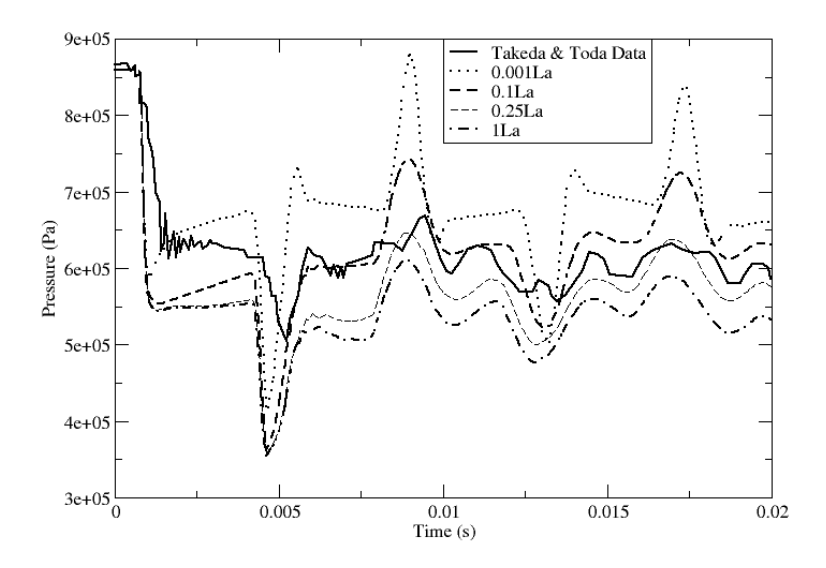


Fig. 15. Laplace Length (bubble radius) effect at PT 3.

The Laplace Length, hence bubble radius, at various positions in the pipe calculated from the RELAP5 default simulation is around 2.3 mm. RELAP5 was designed for transients with much longer durations using steady state two-phase flow regimes. In the present case, the actual bubble radius should be smaller due to the very short time duration of the experiment. The time dependent size of the bubble is initially inertially controlled [13] and can be modeled with the Rayleigh-Plesset equation [14]. However, after a very short critical time thermal effects limit the bubble growth and Plesset-Zwick theory is added to the Rayleigh-Plesset equation [14]. Using the default simulation fluid conditions near the break, the critical time is calculated to be about 80 nanoseconds. The bubble growth, therefore, is namely restricted by thermal effects for the duration of the experiment. The thermal bubble radius *R* is calculated using the Plesset-Zwick [15] theory

$$R = \frac{1}{2C(1/2)} \frac{\rho_f c_{pf} (T_f - T_{sat})}{\rho_g h_{fg}} (\alpha_f t)^{1/2}$$
 (13)

where the value of C(1/2) is calculated to be $\frac{\sqrt{3\pi}}{6}$, c_{pf} is the specific heat at constant pressure of the fluid, h_{fg} is the phasic difference specific enthalpy, and T_{sat} is the saturation temperature.

The bubble radius is calculated with Eq. (13) for 10 ms using the greatest superheat value at a location near the pipe break where the fluid experiences the greatest tension, and the pressure

undershoot is greatest due to the underprediction obtained in the default simulation. Even then, the bubble radius is nearly an order of magnitude less than the 2.3 mm bubble radius used in the RELAP5 simulation. This justifies the use of a 0.1 multiplication factor to be used on the Laplace Length.

2.4 Modified RELAP5 Results

As Fig. 16 demonstrates, the use of a 0.5 subcooled discharge coefficient and a reduction in the bubble diameter by a factor of 10 produces results that match the experimental measurements better than the default model. The discharge coefficient sets the correct initial pressure undershoot and the decrease in bubble diameter produces a better pressure prediction during the rest of the transient. Therefore, two key constitutive relations of the default model that cause significant discrepancies have been identified and the justification for adjusting them to give results closer to the experimental data was given. Finally, Fig. 17 shows the modified pressure distribution. Comparing Fig. 17 with Figs. 5 and 10, this case lies between the equilibrium and default models.

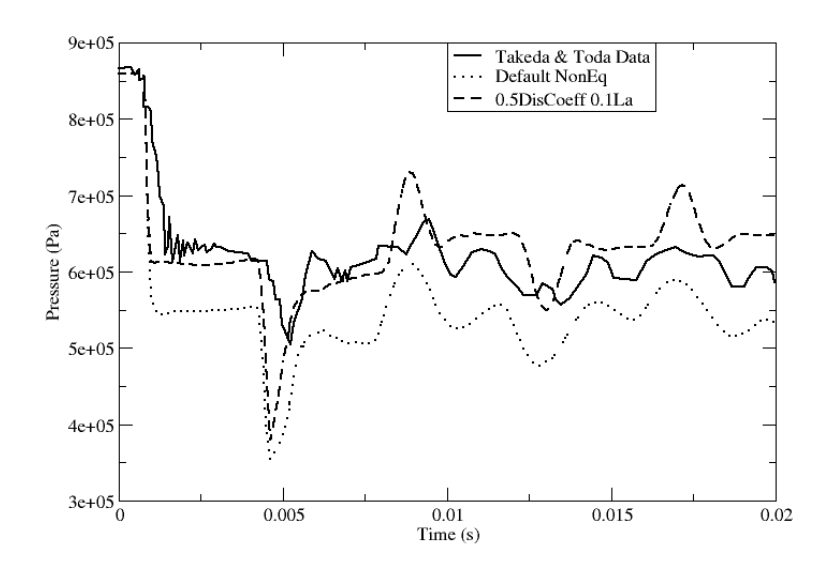


Fig. 16. Simulation with 0.5 discharge coefficient and 0.1 Laplace Length factor at PT 3.

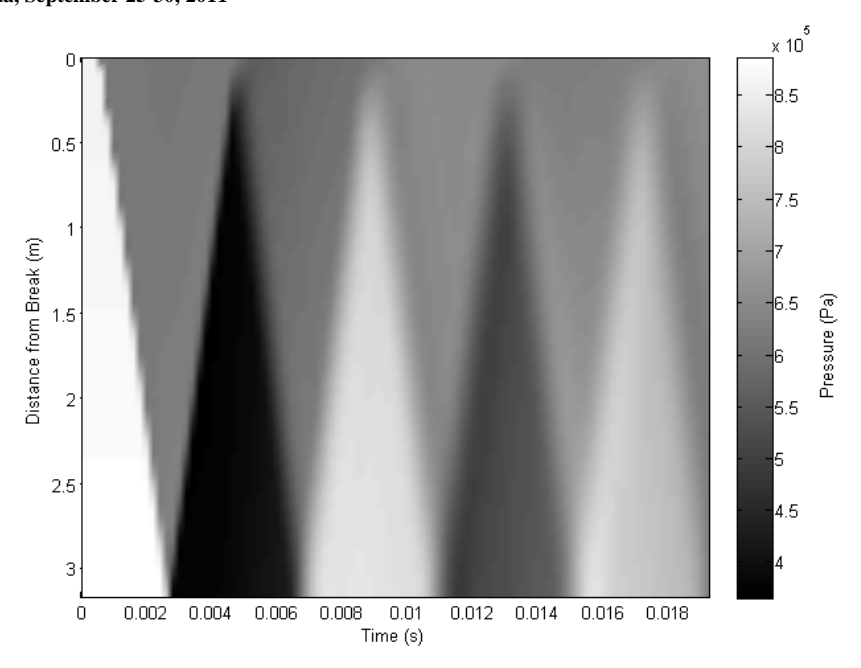


Fig. 17. Pressure (Pa) distribution with time using 0.5 discharge coefficient and 0.1 Laplace Length factor.

3. Stability

Expanding the derivatives in Eqs. (3) and (4), the original system of partial differential equations can be cast into vector equation form

$$\mathbf{A}\frac{\partial \phi}{\partial t} + \mathbf{B}\frac{\partial \phi}{\partial x} = \mathbf{C} \tag{14}$$

where $\underline{\phi} = [\alpha, v_g, v_f, p_{ig}]^T$ is the vector of the independent variables. The coefficient matrices and the source vector \mathbf{C} are obtained from Eqs. (3) and (4) and are not shown. This system of equations must satisfy $\det[\mathbf{A}\lambda - \mathbf{B}] = 0$ for a non-trivial solution to exist. For $v_g = v_f = 0$ Fig. 18 shows that the solutions are $\lambda_{1,4} = 0, 0, +c_{2phase}, -c_{2phase}$, where the first two characteristics are the kinematic wave speeds and the last two characteristics are the acoustic wave speeds given by:

$$c_{2phase} = \sqrt{\frac{\rho_g}{\alpha \rho_f} \frac{c_{vm} \rho_f + (1 - \alpha) \rho'}{c_{vm} \rho' + (1 - \alpha) \rho_f}} c_g, \quad \rho' = \alpha \rho_f + (1 - \alpha) \rho_g$$
 (15)

It is well known [17] that the virtual mass has a significant effect on the two-phase sound speed as shown by Fig. 19 which is a plot of Eq. (15). Drew and Passman [18] have shown that in general (i.e., $v_g \neq v_f \neq 0$) the kinematic roots are real if the two fluid model is complete. In the present problem this is accomplished with the virtual mass coefficients $c_{vm} = 0.5$ for bubbly flow. Furthermore, Fig. 18 shows that the acoustic wave speeds for the RELAP5 model are always real [17] even though the kinematic roots may not be so (i.e., ill-posedness is kinematic). For this particular case the kinematic roots are on the stability boundary. Finally, the energy equations (5) simply add two more

characteristics $\lambda_{5,6} = v_f, v_g$. Therefore the system of equations (3), (4) and (5) is well posed for this case.

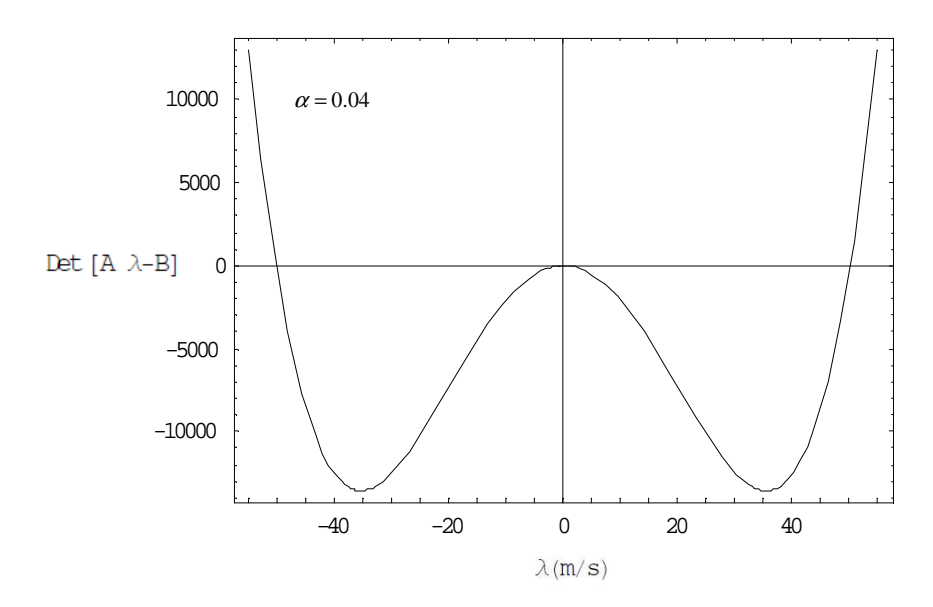


Fig. 18: Characterisitc polynomial vs. wave speed

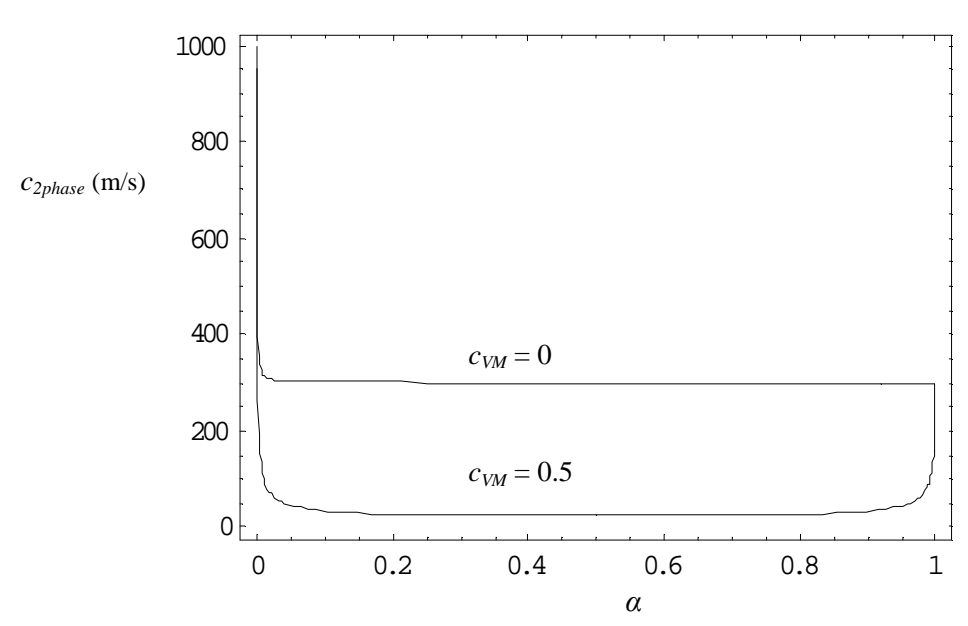


Fig. 19: Two-phase acoustic wave speed

4. Conclusions

RELAP5 simulated a single phase gas shock tube and the results were found in close agreement with an analytic solution. This shows that the numerical uncertainty of RELAP5 is small compared to the uncertainty of the two-phase constitutive relations as demonstrated by the simulation of the two-phase decompression wave experiment of Takeda and Toda. The two phase problem requires the solution of the two-fluid model with many constitutive relations to account for phase change, choked flow, and other pertinent phenomena. In particular RELAP5 captured the details of the reflection of the pressure wave off a sound speed discontinuity between a single-phase and two-phase regions caused by the imposed temperature gradient in the experiment. Two RELAP5 constitutive models that caused significant discrepancies between the model and the data were identified:

- 1. The RELAP5 default model simulation underpredicted the pressure due to low interfacial heat transfer rates because RELAP5 does not have an interfacial area transport model to capture the dynamics of the bubble size. Using the Plesset-Zwick theory during the fast acoustic wave propagation, the average bubble diameter was shown to be one order of magnitude smaller than predicted by RELAP5. A similar observation has been made in a separate research analysis of a water hammer after a fast closing valve using RELAP5 [16]. Clearly, the quasi steady model of RELAP5 is not applicable to acoustic phenomena.
- 2. The choked flow model used by RELAP5 resulted in overpredicting the pressure undershoot. However, this was resolved by altering the discharge coefficient to account for uncertainties in the discharge geometry and/or the choked flow model at low pressure. This correction is attributed only to this experiment and is not meant as a general statement.

The RELAP5 solution with the adjusted bubble diameter and choked flow discharge coefficient matched the experimental data better than the default model. The data obtained from the RELAP5 simulation also proved useful to understand the physics of the experiment. The cause of the dispersion and dissipation of the wave upon reflecting off the two-phase region was identified to be caused by the wave becoming trapped inside a two-phase flow region and the importance of thermal non-equilibrium and the delay in bubble nucleation became evident by the investigation of the RELAP5 results. Therefore, RELAP5 proved to be a useful heuristic tool.

5. References

- [1] Edwards, A R and O'Brien, T P., Studies of Phenomena Connected with the Depressurization of Water Reactors. Journal of the British Nuclear Energy Society, 1970, pp. 125-35.
- [2] Takeda, Y and Toda, S., *Pressure Oscillation in Subcooled Decompression under Temperature Gradient*. Journal of Nuclear Science and Technology, 1979, pp. 484-495.
- [3] Information Systems Laboratories, Inc., *RELAP5/MOD3.3 CODE MANUAL VOLUME I VIII*. Rockville, MD and Idaho Falls, ID , 2006.
- [4] Tiselj, I and Cerne, G., *Some Comments on the Behavior of the RELAP5 Numerical Scheme at Very Small Time Steps*, Nuclear Science and Engineering, 2000, p. 306.
- [5] Shapiro, A. *The Dynamics and Thermodynamics of Compressible Fluid Flow, Vol 2.* Ronald Press Co., 1954.
- [6] Pokharna, H, Mori, M and Ransom, V., Regularization of Two-Phase Flow Models: A Comparison of Numerical and Differential Approaches. Journal of Computational Physics, Vol. 134, 1997, pp. 282-295.
- [7] Ivashneva, M, Ivashnyov, O and Smirnov, N., Slow Waves of Boiling Under Hot Water Depressurization. Journal of Fluid Mechanics, 2000, pp. 149-180.
- [8] Davis, J., Mathematics of Wave Propagation. Princeton University Press, 2000.
- [9] Trapp, J and Ransom, V., A Choked-Flow Calculation Criterion for Nonhomogeneous, Non-equilibrium, Two-Phase Flows. International Journal of Multiphase Flow, 1982, pp. 669-681.
- [10] Alamgir, M and Lienhard, J., Correlation of Pressure Undershoot During Hotwater Depressurization. Journal of Heat Transfer, Transactions ASME, 1981, 103(1): pp. 52–55.
- [11] Ishii, M. Argonne National Laboratory, private communication, letter to R. Nelson. July 1987.
- [12] Los Alamos National Laboratory, *TRAC-M/FORTRAN 90 (VERSION 3.0) THEORY MANUAL*. Los Alamos, NM; University Park, PA, 2000. la-ur-00-910 edition.
- [13] Ghiaasiaan, M., Two-Phase Flow, Boiling, and Condensation in Conventional and Miniature Systems. New York: Cambridge University Press, 2008.
- [14] Brennen, C., Cavitation and Bubble Dynamics. New York: Oxford University Press, 1995.
- [15] Plesset, M and Zwick, S., *The Growth of Vapor Bubbles in Superheated Liquids*. Journal of Applied Physics, 1954, pp. 493-500.
- [16] Barten, W, Jasiulevicius, A, Manera, A., Analysis of the Capability of System Codes to Model Cavitation Water Hammers: Simulation of UMSICHT Water Hammer Experiments with TRACE and RELAP5, Nuclear Engineering and Design, 2008, 238, 4, pp. 1129-1145.
- [17] Stadtke, H., Gasdynamic Aspects of Two-Phase Flow: Hyperbolicity, Wave Propagation Phenomena, and Related Numerical Methods, Wiley-VCH, Weinheim, Germany, 2006.
- [18] Drew, D.A. and Passman, S.L., *Theory of multicomponent fluids*, Applied Mathematical Sciences. Springer, Berlin, 1998.